RSC Advances

PAPER

View Article Online
View Journal | View Issue

Cite this: *RSC Adv.*, 2024, **14**, 5812

Charge transport mechanisms of $PbSnSe_2$ and observation of transition from direct to Fowler–Nordheim tunneling

Qaisar Abbas,[a] Syed Mesam Tamar Kazmi,[a] Chuanbo Li,[b] Xiulai Xu [cd] and M. A. Rafiq [*a]

Received 15th November 2023
Accepted 26th January 2024

DOI: 10.1039/d3ra07812d

rsc.li/rsc-advances

In this study, we report the observation of various conduction mechanisms in mechanically exfoliated $PbSnSe_2$ based on temperature-dependent current and voltage characteristics. A transition from direct tunneling to Fowler–Nordheim tunneling in $PbSnSe_2$ was observed at 2.63 V. At lower temperatures, the 3D Mott variable range hopping model fits the data, yielding a density of states of $\sim 8.80 \times 10^{20}$ eV^{-1} cm^{-3} at 2 V. The values of W_{hop} and R_{hop} were 64 meV and 22.7 nm, respectively, at 250 K. The Poole–Frenkel conduction was observed in the Au/$PbSnSe_2$/Au device and the dielectric constant of $PbSnSe_2$ was calculated to be 1.4. At intermediate voltages, a space charge limited current with an exponential distribution of traps was observed and a trap density of $\sim 9.53 \times 10^{13}$ cm^{-3} and a trap characteristic temperature of 430 K were calculated for the Au/$PbSnSe_2$/Au device.

Introduction

Ever since the successful isolation of monolayer graphene, which has intrinsic bandgap limitations, the quest for novel van der Waals materials exhibiting remarkable electronic properties has become an unceasing pursuit.[1] In this relentless exploration, the metal chalcogenide family is the most well studied after graphenes, but large strides are made on other materials as well.[2] Among these materials, group-IV monochalcogenides (MX: M = Pb and Sn and X = S, Se, and Te) have shown great potential in the fields of nanoelectronics,[3] optoelectronics,[4] sensors,[5] catalysis,[6] energy storage,[7] and thermoelectric devices[8] owing to their high carrier mobilities, high on/off ratios, tunable band structures, and excellent thermoelectric properties. Moreover, their low cost and earth abundance are considered ancillary advantages to other traits.[9] $PbSnSe_2$ is a ternary compound of group IV metal chalcogenides poised to unravel new paradigms in the field of nanoelectronics. Only a few computational studies have been reported on this material;[10–12] however, experimental studies on $PbSnSe_2$ have been overlooked.

Therefore, we report the observations of various conduction mechanisms in mechanically exfoliated $PbSnSe_2$ from the temperature-dependent current and voltage (*IV*) characteristics. A transition from direct tunneling (DT) to Fowler–Nordheim tunneling (FN) in $PbSnSe_2$ was observed at 2.63 V. At lower temperatures, the Mott variable range hopping (VRH) model fits the experimental data well, yielding the Mott characteristic temperature, density of states, hopping distance, and average hopping energy of the charge carriers in $PbSnSe_2$. Moreover, the dielectric constant of $PbSnSe_2$ was approximated from the Poole–Frenkel emission at higher voltages. Subsequently, using the space charge limited current (SCLC) model, we evaluated the trap density using the crossover voltage and calculated the characteristic temperature and energy of these traps.

Experimental details

Pure $PbSnSe_2$ crystals (purchased from Six Carbon Technology) were exfoliated using thermal release tape and transferred onto a silicon substrate with a thin layer of SiO_2. The chosen flake of $PbSnSe_2$ with a lateral size of ~5 μm was then transferred to interdigitated electrodes (IDEs), as shown schematically in Fig. 1a, along with the optical image. IDE consisted of 10 comb-like pairs of gold electrodes 5 μm apart on a glass substrate. The temperature-dependent *IV* characteristics were recorded using an Agilent semiconductor parameter analyzer 4156C in a cryogenic probe station.

Results and discussion

Fig. 1b shows the temperature-dependent nonlinear *IV* characteristics of $PbSnSe_2$ from 150 K to 250 K. The inset of Fig. 1b shows that the switching in $PbSnSe_2$ flakes is $\sim 10^5$. This switching in Au/$PbSnSe_2$/Au devices may find applications in $PbSnSe_2$-based high-voltage resistive switching devices.[13] As can

[a]*Condensed Matter Physics Laboratories, Department of Physics and Applied Mathematics, Pakistan Institute of Engineering and Applied Sciences, PO Nilore, Islamabad 45650, Pakistan. E-mail: aftab@cantab.net*
[b]*School of Science, Minzu University of China, Beijing 100081, China*
[c]*Institute of Physics, Chinese Academy of Sciences, Beijing 100190, China*
[d]*State Key Laboratory for Mesoscopic Physics and Frontiers Science Center for Nano-optoelectronics, School of Physics, Peking University, Beijing 100871, China*

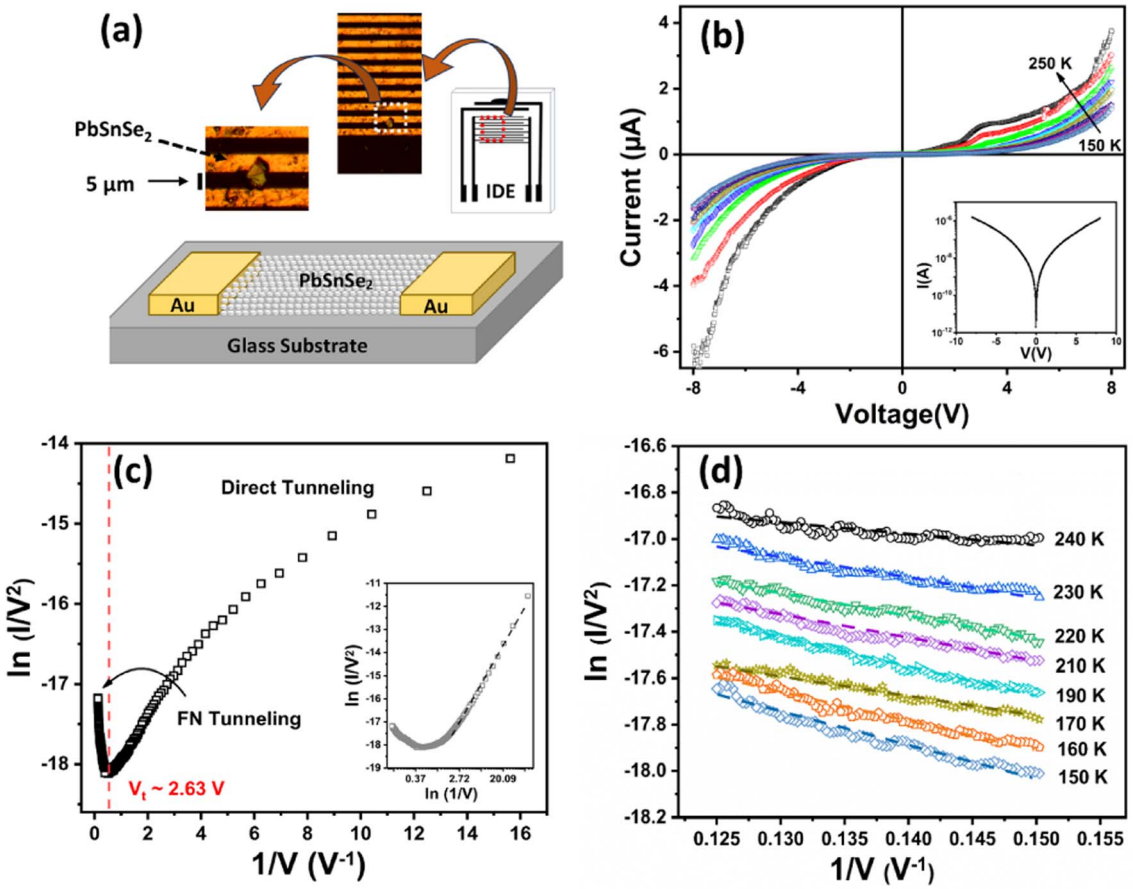

Fig. 1 (a) Schematic and optical image of $PbSnSe_2$ flakes on gold contacts 5 μm apart on a glass substrate. (b) Temperature-dependent *IV* characteristics of $PbSnSe_2$ flakes in the temperature range of 150–250 K. (c) $\ln(I/V^2)$ and $1/V$ showing the transition between FN tunneling and direct tunneling at a transition voltage of ~2.63 V. The inset shows the plot of $\ln(I/V^2)$ and $\ln(1/V)$ confirming the linear fit of direct tunneling. (d) $\ln(I/V^2)$ and $\ln(1/V)$ showing the linear fits of FN tunneling at different temperatures.

be seen from Fig. 1b, the flake exhibits semiconducting behaviors. Xu *et al.*[10] have shown that $PbSnSe_2$ exhibits semiconducting behaviors if the number of layers in the flake is less than 8. Therefore, we suggest that the number of layers in the flake should be less than 8.

Fig. 1c shows the $\ln(1/V^2)$ *vs.* $1/V$ plot of the $PbSnSe_2$ device at 220 K. This plot shows the change in behavior at a particular voltage at all temperatures. This change is observed at $1/V \approx 0.38\ V^{-1}$ (2.63 V), which segregates the plot into two distinct regions. These two regions correspond to FN tunneling and DT. When the externally applied voltage is smaller in magnitude than the barrier height, DT occurs, which corresponds to the tunneling of charge carriers through a trapezoidal barrier. In contrast, for voltages exceeding the barrier height, electrons tunnel through a triangular barrier, *i.e.*, FN tunneling occurs, which is analogous to field emission. The tunneling current can be expressed using the following relation:[14]

$$I \propto \begin{cases} V \exp\left(-\dfrac{2d\sqrt{2m^*\varphi}}{\hbar}\right) (V < V_t) : \text{Direct tunneling} \\ V^2 \exp\left(-\dfrac{4d\sqrt{2m^*\varphi^3}}{3\,\hbar e V}\right) (V > V_t) : \text{FN tunneling} \end{cases} \quad (1)$$

where e is the charge on electron, $\hbar$ is Planck's constant, d is the distance between the electrodes, m^* is the effective mass of an electron and φ is the barrier height.

Using eqn (1), the fitted curves showed excellent agreement with the experimental data. The term $\ln(I/V^2)$ exhibits a linear decrease at high voltages, which refers to FN tunneling. The logarithmic growth at low voltages implies that direct tunneling is the dominant transport mechanism in this region. The average value of the transition voltage was calculated to be approximately 2.63 V. Therefore, the barrier height is 2.63 eV according to the formula $V_t = \varphi/e$ for the Au/$PbSnSe_2$/Au device.[15]

Fig. 2a shows the Arrhenius plot for studying the two different transport mechanisms: at high temperatures, thermally activated transport mechanism, whereas at low temperatures, data fit Mott's three-dimensional VRH model, as shown in Fig. 2b. This model obeys the following equation:[16]

$$G = G_0 \exp\left[-\left(\frac{T_0}{T}\right)\right]^{\frac{1}{4}} \quad (2)$$

The pre-exponential factor G_0 weakly depends on the temperature, and T_0 is the Mott temperature related to the

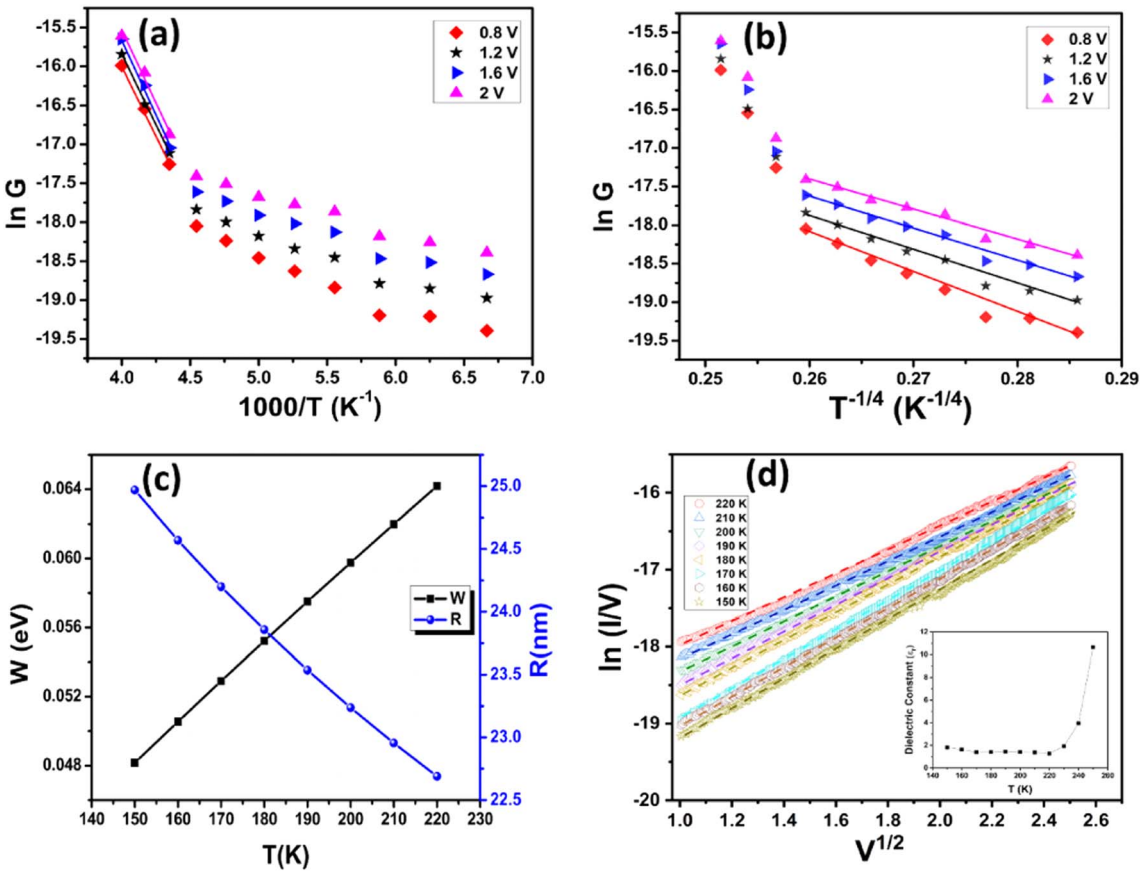

Fig. 2 (a) Plots of ln G *vs.* 1000/T and (b) ln G *vs.* $T^{-0.25}$ with the linear fit showing the thermally activated region and 3D Mott VRH region respectively at different voltages. (c) Behavior of average hopping energy W_H and average minimum hopping distance R_{min} with temperature. (d) ln(I/V) *vs.* $V^{1/2}$ for the Poole–Frenkel emission at different temperatures; the inset shows the values of dielectric constant.

density of localized states whose relation is given by the following equation:[17]

$$T_0 = \frac{24}{\pi k_B N(E_F)\alpha^3} \quad (3)$$

where α is the localization length and $N(E_F)$ is the density of localized states. The presence of Mott VRH may be explained as follows: the flakes of layered structures such as graphenes, transition metal chalcogenides, and their ternary compounds have a certain degree of defects or disorders. These defects are the reason for the formation of localized electronic states. Charge carriers navigate through hopping between these localized states when the carrier density is low.[18] The values of the characteristic temperature T_0 were calculated from the slopes of the fitted curves, as shown in Fig. 2b. The density of localized states was estimated by assuming the value of $\alpha = 0.351$ nm and using the value of T_0 extracted from the experimental data. The calculated values of T_0 and $N(E_F)$ at different voltages are shown in Table 1.

Mott's VRH parameters also include the hopping distance (R_{hop}) and the hopping energy (W_{hop}), which were calculated using the following equations:[17]

$$R_{hop} = \left[\frac{\alpha}{8\pi N(E_F)k_B T}\right]^{1/4} \quad (4)$$

and

$$W_{hop} = 0.25 k_B T \left(\frac{T_0}{T}\right)^{1/4} \quad (5)$$

The graph is plotted for R_{hop} and W_{hop} as a function of temperature, as shown in Fig. 2c. The decrease in the values of hopping distance is due to the increase in the disorder of the system with temperature.[19] This leads to the conduction by hopping of carriers from states located closely in space to the

Table 1 Characteristic temperature T_0 and density of localized states $N(E_F)$ of $PbSnSe_2$ flakes at different voltages in the temperature range of 150 K–230 K

Voltage (V)	T_0 (K)	$N(E_F)$ (eV^{-1} cm^{-3})
0.8	7.38 × 106	2.76 × 10^{20}
1.2	3.65 × 106	5.58 × 10^{20}
1.6	2.96 × 106	6.87 × 10^{20}
2.0	2.31 × 106	8.80 × 10^{20}

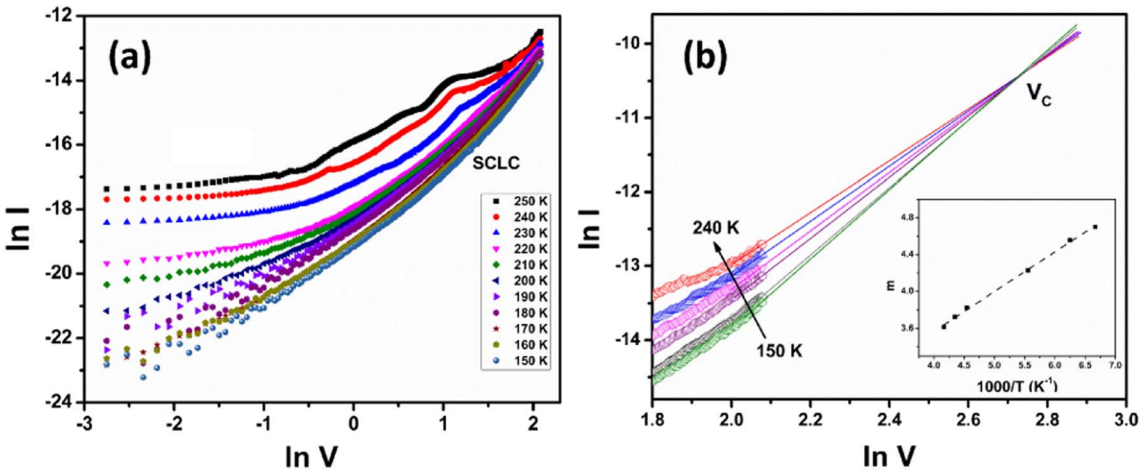

Fig. 3 (a) *IV* characteristics on a double logarithmic graph to illustrate the presence of SCLC behavior at high voltages. (b) Linear extrapolation at higher voltages meets at a crossover voltage of 15.39 V. The inset shows the linear fit of slope *m vs.* 1000/*T*.

initial state. In contrast, the hopping energy tends to increase with the increase in temperature. This is due to the fact that the increase in disorder requires extra energy for the carriers to make a transition from the initial to the final state.[19]

Fig. 2d shows that data at higher voltages obey the $\ln(\sigma)$ *vs.* V dependence, which is Poole–Frenkel emission. It refers to the thermal excitation of charge carriers trapped inside a potential well that are enhanced by an electric field. Conduction through the PF mechanism is given as follows:[20]

$$I \sim V \exp\left(\frac{\beta_{PF}\sqrt{V} - \varphi_{PF}}{k_B T}\right) \quad (6)$$

where φ_{PF} is the barrier height and β_{PF} is the barrier lowering. It is evident from Fig. 2d that the data can be fitted through a straight line, which indicates that PF emission follows the dominant conduction mechanism. Additionally, the dielectric constant of the material can be extracted from the slope of the $\ln(I/V)$ *vs.* V curves. In the PF emission, *IV* curves obtained from the $PbSnSe_2$ flake have a slope related to the dielectric constant ε_r by the following relation:[21]

$$S = \frac{\sqrt{\frac{q^3}{d\pi\varepsilon_0\varepsilon_r}}}{k_B T} \quad (7)$$

The inset of Fig. 2d shows that the value of the dielectric constant for $PbSnSe_2$ in the temperature range of 150 K–220 K is approximately 1.4, which is much close to the values of the dielectric constant found for the ternary compound.[10]

Fig. 3a shows the *IV* characteristics on a double logarithmic scale at intermediate voltages (150 K–250 K). The estimated values of the slopes vary in the range of ~3–5. The values of slope increase while moving towards lower temperatures because the trapped electrons become more stable.[22] A slope greater than two infers the presence of SCLC with an exponential distribution of traps and is given as follows:[23]

$$J = q^{l-1}\mu N_{DOS}\left(\frac{2l+1}{l+1}\right)^{l+1}\left(\frac{l}{l+1}\frac{\varepsilon_r\varepsilon_0}{N_t}\right)^{l}\frac{V^{l+1}}{d^{2l+1}} \quad (8)$$

where N_t is the trap density, N_{DOS} is the density of states in the relevant band, μ is the charge carrier mobility, q is the electronic charge, ε_r is the dielectric constant of the material, ε_o is the permittivity of free space, and d is the distance between the two electrodes. The factor l is equal to T_t/T, where T_t is the characteristic temperature and T is the temperature at which the particular measurement is taken. Eqn (5) clearly depicts that the power law of the form $I \propto V^m$ holds with the factor $m = l + 1$.

Fig. 3b shows the $\ln I$–$\ln V$ graph, which meets at a specific point after extrapolating the lines and this single point is referred to as "cross-over voltage (V_c)". The relation of V_c with the trap density is given by the following equation:[19]

$$V_c = \frac{qN_t d^2}{2\varepsilon_r\varepsilon_0} \quad (9)$$

From Fig. 3b, the cross-over voltage for $PbSnSe_2$ flakes comes out to be 15.39 V. Using the value of $\varepsilon_r = 1.4$ and V_c in eqn (6), the trap density comes out to be 9.53×10^{13} cm^{-3}. The inset of Fig. 3b illustrates that m increases linearly as a function of the inverse temperature, which is in agreement with the SCLC model. The characteristic temperature T_t comes out to be ~430 K, which leads to a characteristic energy of 37 meV.

Conclusions

In summary, a transition from direct tunneling to FN tunneling in an Au/$PbSnSe_2$/Au device was observed at 2.63 V. The values of $N(E_F)$ estimated using the 3D Mott VRH model ($p = 1/4$) were found to be 2.76×10^{20} to 8.80×10^{20} eV^{-1} cm^{-3} at 0.8 to 2 V, respectively. Moreover, the values of W_{hop} and R_{hop} were calculated to be 48 meV and 25 nm, respectively, at 150 K. Whereas at 220 K, the values of W_{hop} and R_{hop} were 64 meV and 22.7 nm, respectively. The data fitting proved that Poole–Frenkel emission is the dominant conduction mechanism, which

led to the calculation of the dielectric constant (~1.4). At intermediate voltages, SCLC with an exponential distribution of traps was observed in the Au/$PbSnSe_2$/Au device, and from this model, the trap density turned out to be ~9.53×10^{13} cm^{-3}. Moreover, the characteristic trap temperature and energy of this device were calculated to be 430 K and 37 meV, respectively.

Data availability

Data sharing is not applicable to this article as no new data were created or analysed in this study.

Author contributions

Qaisar Abbas: investigation (equal); writing – original draft (equal); writing – review and editing (equal). Syed Mesam Tamar Kazmi: investigation (equal); writing – original draft (equal); writing – review & editing (equal). Chuanbo Li: investigation (supporting); resources (equal). Xiulai Xu: investigation (supporting); resources (equal). M. A. Rafiq: investigation (equal); writing – original draft (equal). writing – review & editing (equal); resources (equal); supervision (equal).

Conflicts of interest

The authors have no conflicts of interest to disclose.

References

1 R. Frisenda, Y. Niu, P. Gant, M. Muñoz and A. Castellanos-Gomez, *npj 2D Mater. Appl.*, 2020, **4**, 38.
2 S.-L. Li, K. Tsukagoshi, E. Orgiu and P. Samorì, *Chem. Soc. Rev.*, 2016, **45**, 118–151.
3 W. Prost, F. Kruis, F. Otten, K. Nielsch, B. Rellinghaus, U. Auer, A. Peled, E. Wassermann, H. Fissan and F. Tegude, *Microelectron. Eng.*, 1998, **41**, 535–538.
4 K. V. Chandekar, F. H. Alkallas, A. B. G. Trabelsi, M. Shkir, J. Hakami, A. Khan, H. E. Ali, N. S. Awwad and S. AlFaify, *Phys. B*, 2022, **641**, 414099.
5 A. Munoz, J. Melendez, M. Torquemada, M. Rodrigo, J. Cebrian, A. De Castro, J. Meneses, M. Ugarte, F. López and G. Vergara, *Thin Solid Films*, 1998, **317**, 425–428.
6 Z. Tachan, M. Shalom, I. Hod, S. Ruhle, S. Tirosh and A. Zaban, *J. Phys. Chem. C*, 2011, **115**, 6162–6166.
7 S. Majumder, S. Karade, R. Kumar, M. Gu, B. R. Sankapal and K. H. Kim, *J. Alloys Compd.*, 2022, **906**, 164323.
8 W. Liang, O. Rabin, A. I. Hochbaum, M. Fardy, M. Zhang and P. Yang, *Nano Res.*, 2009, **2**, 394–399.
9 L. C. Nhan, V. T. T. Vi, D. X. Du, N. Q. Cuong, N. N. Hieu and T. P. T. Linh, *Chem. Phys.*, 2023, **566**, 111797.
10 W. Xu, Z. Xie, J. Su, R. Wang, X. Wu and H. Xu, *J. Phys. Chem. Lett.*, 2021, **12**, 10574–10580.
11 T. Wang, X. Duan, H. Zhang, J. Ma, H. Zhu, X. Qian, J. Y. Yang, T. H. Liu and R. Yang, *InfoMat*, 2023, e12481.
12 C.-H. Ding, Z.-F. Duan, N.-N. Luo, J. Zeng, W. Ren, L.-M. Tang and K.-Q. Chen, *Nanomaterials*, 2023, **13**, 1519.
13 S. Pandey, C. Biswas, T. Ghosh, J. J. Bae, P. Rai, G.-H. Kim, K. J. Thomas, Y. H. Lee, P. Nikolaev and S. Arepalli, *Nanoscale*, 2014, **6**, 3410–3417.
14 J. M. Beebe, B. Kim, J. W. Gadzuk, C. Daniel Frisbie and J. G. Kushmerick, *Phys. Rev. Lett.*, 2006, **97**, 026801.
15 T. Ikuno, H. Okamoto, Y. Sugiyama, H. Nakano, F. Yamada and I. Kamiya, *Appl. Phys. Lett.*, 2011, **99**, 023107.
16 N. F. Mott, *Philos. Mag.*, 1969, **19**, 835–852.
17 L. Zhang and Z.-J. Tang, *Phys. Rev. B: Condens. Matter Mater. Phys.*, 2004, **70**, 174306.
18 Q. Liang, Q. Zhang, X. Zhao, M. Liu and A. T. S. Wee, *ACS Nano*, 2021, **15**, 2165–2181.
19 Z. Imran, M. A. Rafiq and M. M. Hasan, *AIP Adv.*, 2014, **4**, 067137.
20 M. Choueib, A. Ayari, P. Vincent, S. Perisanu and S. Purcell, *J. Appl. Phys.*, 2011, **109**, 073709.
21 J. R. Yeargan and H. L. Taylor, *J. Appl. Phys.*, 2003, **39**, 5600–5604.
22 M. Rafiq, Y. Tsuchiya, H. Mizuta, S. Oda, S. Uno, Z. Durrani and W. Milne, *Appl. Phys. Lett.*, 2005, **87**, 182101.
23 S. M. T. Kazmi, Z. Zahoor, N. T. Yusra, M. H. Bhatti, M. F. Afsar, F. Sher, H.-u. Rashid and M. A. Rafiq, *Phys. B*, 2023, **670**, 415400.